MRS Communications (2020), *10*, 512–518

doi:10.1557/mrc.2020.59

MRS Communications

Research Letter

Effect of poly(dimethylsiloxane) binder in a silica-based superhydrophobic coating on mechanical properties, surface roughness, and wettability

Divine Sebastian and **Chun-Wei Yao**, Department of Mechanical Engineering, Lamar University, Beaumont, TX 77710, USA
Address all correspondence to Chun-Wei Yao at **cyao@lamar.edu**

(Received 11 June 2020; accepted 27 July 2020)

Abstract

This work investigates the influence of poly(dimethylsiloxane) (PDMS) within a nanocomposite coating solution constituted by silica nanoparticles and toluene on mechanical properties, surface wettability, and surface morphology. The developed coating's hardness and elastic modulus were studied in detail. A variation in mechanical properties was observed as the amount of PDMS was varied. Also, the average surface roughness, skewness, and kurtosis values show the influence of the amount of PDMS on the surface roughness characteristics of the coating. Furthermore, it was observed that the water contact angles were linked with the proportion of PDMS.

Introduction

Superhydrophobic coatings have been a hot topic for the research community since the last few decades because superhydrophobicity has many applications, which include but are not limited to anticorrosion,[1,2] self-cleaning,[3] and anticing.[4] Various methods exist for fabricating a superhydrophobic coating; these include the sol–gel method,[5] chemical vapor deposition,[6] physical vapor deposition,[7] and a nanocomposite solution.[8–12] Varied in their complexity, fabrication methods are selected according to which a basic substrate is to be coated and which chemicals are to be used. The basic requirements for developing a superhydrophobic coating are low surface free energy (surface chemistry)[13] and considerably higher surface roughness (surface morphology).[14] So, any fabrication technique, irrespective of its nature, includes distinct processing steps to alter these properties of surface chemistry and morphology to enhance superhydrophobic behavior. The one exception to this, out of the previously mentioned techniques, is the nanocomposite coating solution, as it can achieve the desired alterations in a single coating process.[15] Generally, a nanocomposite solution comprises nanoparticles such as silica or nanoparticles of varying sizes, a binder such as poly(dimethylsiloxane) (PDMS), and an appropriate solvent medium such as toluene or ethanol.[15] The nanoparticles are responsible for the required surface morphology. If they are functionalized prior to use to reduce surface free energy, they could also affect the required surface chemistry.[16] The role of the binder is to hold the constituents together, thereby achieving the desired mechanical properties rendering the coating durable.[17]

One of the main problems associated with superhydrophobic coatings is their susceptibility to damage by external wear and abrasion; this susceptibility is often caused by insufficient mechanical properties.[18] When it comes to nanocomposite coating solutions, since the binding agent is responsible primarily for holding the coating firmly and stably onto the substrate, it might seem possible to improve the mechanical properties of the coating simply by increasing the amount of binding medium within the nanocomposite coating solution. PDMS, with its considerable adherence and abrasion resistance, is often used as a binder medium within nanocomposite solutions,[17,19] and it is the binder used in this work. Many past studies have tried to study the influence of the degree of cross-linking within PDMS on its mechanical properties.[20–22] When PDMS is used as a binder within a nanocomposite coating, researchers have also investigated the influence of varying the number of nanoparticles in the nanocomposite coating while keeping the amount of PDMS constant. Bolvardi et al. revealed that in a nanocomposite coating composed of titania nanoparticles and PDMS, superhydrophobicity was significantly decreased by increasing the number of nanoparticles.[23] Bolvardi et al. also found that PDMS played a vital role in achieving the desired surface properties for the same titania-based nanocomposite coating. Amirpoor et al. studied the influence of silica and PDMS on the oil–water separation efficiency of a superhydrophilic/superoleophobic nanocomposite coating where the amount of PDMS was kept constant.[24] Their results revealed that PDMS and the change in the number of nanoparticles had a considerable influence on the oil contact angle of the nanocomposite coating. With respect to the number of nanoparticles, the highest oil contact angle was obtained when the number of nanoparticles was highest, whereas with respect to PDMS, the highest oil contact angle was obtained when the amount of PDMS was lowest. To investigate the

possibility of improving the mechanical properties and other significant properties of a nanocomposite coating with PDMS as the binder, a nanocomposite coating solution using silica nanoparticles, PDMS, and toluene is studied in this work by varying the amount of PDMS. After a series of experiments, the weight proportions of the chemical constituents were optimized for the selected nanocomposite solution. The only parameter varied here is the amount of PDMS within the nanocomposite solutions. With the aid of nanoindentation, the dependence of mechanical properties such as the coating's hardness and elastic modulus on the amount of PDMS within the nanocomposite coating solution was accurately measured. The work also studied variation in surface roughness and surface wettability with respect to the change in the amount of PDMS to investigate the influence of the amount of PDMS on these characteristic properties. Surface wettability was quantified by the static contact angle. Surface roughness was quantified with different roughness parameters such as average surface roughness, root-mean-square surface roughness, surface skewness, and kurtosis.

Materials and methods

2024-T3 aluminum alloy plates of 2.5 cm × 2.5 cm × 0.5 mm were used as the substrates. Chemicals used were anhydrous ethanol (Sigma-Aldrich, St. Louis, MO, USA), isopropyl alcohol (Sigma-Aldrich, St. Louis, MO, USA), acetone (Sigma-Aldrich, St. Louis, MO, USA), silane-modified hydrophobic silica nanoparticles (RX-50) with an average diameter of 55 ± 15 nm (Evonik, Piscataway, NJ, USA), toluene (Sigma-Aldrich, St. Louis, MO, USA), polydimethylsiloxane elastomer kit (Sylgard 184) (Dow Corning, Midland, MI, USA). All the experiments were performed at an ambient temperature of 25 °C.

The flat substrates with the given dimensions were cleaned in a sequential manner as follows: ultrasonication in acetone was performed for 15 min followed by thorough rinsing with isopropyl alcohol, ethanol, and deionized water to remove any surface contaminants or grease. This step was followed by drying in air. After the preparation of substrates to be coated, the nanocomposite coating solution was prepared according to the following procedure. 1.5 g of silica nanoparticle was mixed in 6 g of toluene and then the suspension of nanoparticles in toluene was dispersed by ultrasonic stirring for 1 h. Ultrasonication for substantially longer duration is necessary for avoiding aggregation of nanoparticles and to facilitate proper dispersion. Simultaneously, an appropriate amount of PDMS base polymer was added to 4 g of toluene for different nanocomposite solutions and was dispersed by ultrasonic stirring for 1 h. For nanocomposite solution-A, nanocomposite solution-B, nanocomposite solution-C, and nanocomposite solution-D; 0.5, 1.0, 1.5, and 2.0 g of PDMS base polymer were used, respectively. After 1 h, both the solutions were mixed together and continued the ultrasonication for another hour. After this step, the solution was mixed further using a mechanical stirrer for 2 h to ensure better mixing and dispersion. Once the mechanical stirring was performed for 2 h; nanocomposite solution-A, nanocomposite solution-B, nanocomposite solution-C, and nanocomposite solution-D were mixed with 0.05, 0.10, 0.15, and 0.20 g of curing agent, respectively, and the mixture was stirred using mechanical stirrer for another 30 min. The obtained solution was degassed in a vacuum desiccator for 20 min to remove any air bubbles entrapped within the nanocomposite solution. The nanocomposite solutions thus obtained were then deposited on the aluminum alloy substrates using spin coating at a speed of 800 rpm for 10 s. The coating was then oven-cured at 110 °C for 20 min followed by air cooling in a fume hood. The coating obtained using nanocomposite solution-A is hereon referred to as coating-A, and similarly, coating obtained using nanocomposite solution-B, nanocomposite solution-C, and nanocomposite solution-D will be referred to as coating-B, coating-C, and coating-D respectively.

Nanoindentation was performed using a nanoindenter (Hysitron TI 980, Bruker) equipped with a diamond Berkovich tip. The indentations required for the modulus mapping and hardness mapping on the fabricated coatings were carried out using load-controlled quasi-static trapezoidal load function with a peak load of 250 mN. The measurement of static contact angles was performed using a drop shape analyzer (DSA25E, Krüss) to analyze the wetting behavior of different coatings. Deionized water droplets (10 μL) were dropped onto the surfaces under ambient temperature and atmosphere. For each static contact angle measurement, at least four measurements were performed at arbitrarily selected locations on the sample. The surface topographies of the samples were measured using an atomic force microscope (AFM, Park NX10, Park System Co.) in contact mode with a scan area of 10 × 10 μm^2.

Results and discussion

Mechanical property analysis using nanoindentation

To measure the mechanical properties such as reduced elastic modulus and hardness for all the coatings, mapping of those properties was performed over an area of 2 mm × 2 mm. The mapping was achieved by compiling the property values obtained from a matrix of indentations positioned with a gap of 100 μm between successive indentations. A total of 400 indentations were performed for one test, and identical indentations were performed on all the points using a load-controlled trapezoidal quasi-static load function with 250 mN peak load. Figures 1(a)–1(d) show the hardness mapping for coating-A, coating-B, coating-C, and coating-D. Determination of hardness is crucial in quantifying the mechanical stability of coatings, as it gives information about resistance to deformation.[25] It can be observed that, in the case of each coating, the hardness value varies slightly from one location to another. The average hardness for coating-A was 0.20 GPa, whereas that of coating-B, coating-C, and coating-D were 0.11, 0.05, and 0.04 GPa, respectively. The highest hardness value among all the coatings was observed on coating-A, and the lowest value was observed

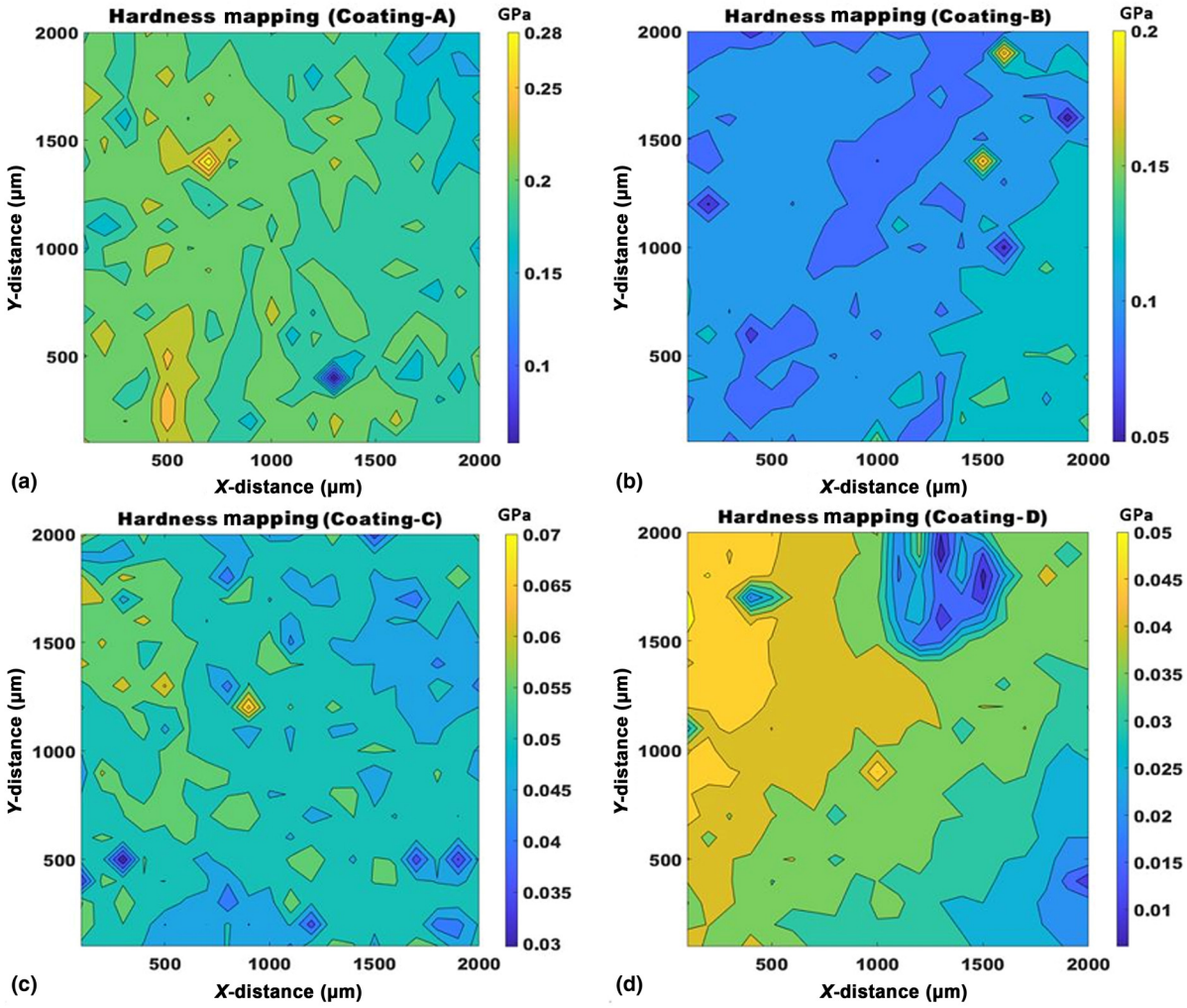

Figure 1. Hardness mapping for (a) coating-A, (b) coating-B, (c) coating-C, and (d) coating-D.

on coating-D, owing to the highest proportion of PDMS within the nanocomposite. These mappings show that the hardness of the coating is inversely proportional to the amount of PDMS within the nanocomposite solution when the levels of all other constituents remain unaltered. Figures 2(a)–2(d) show the reduced elastic modulus mapping for coating-A, coating-B, coating-C, and coating-D. Reduced elastic modulus quantifies the cumulative effect of the elastic deformations.[26] As the same indenter tip and identical loading conditions are used for different coatings in this work, reduced elastic modulus can be effectively used to compare different coatings based on the elastic deformations occurring on them. Similar to the observations made for hardness mapping, the highest modulus value among all the coatings was observed for coating-A, as expected, and the lowest value was observed on coating-D. The average reduced elastic modulus for coating-A was 2.66 GPa, whereas that of coating-B, coating-C, and coating-D were 2.32, 1.59, and 1.24 GPa, respectively. These mappings show that, when the levels of all other constituents besides PDMS remain unaltered, the reduced modulus of the coating is inversely proportional to the amount of PDMS within the nanocomposite solution. Supplementary Table S1 summarizes the average for the values of the reduced elastic modulus and hardness for the 400 distinct indentation points along with the standard deviation. This matrix of indentations was repeated over three samples, and similar results were obtained.

Surface wettability analysis using goniometry

Considering the role of nanoparticles and the binding agent such as PDMS within a nanocomposite solution intended to fabricate superhydrophobic coatings, it is clear that the proportion between the constituents within the nanocomposite solution should be well balanced and optimized in order to achieve desirable wetting behavior. Since surface morphology and surface chemistry of the fabricated coating are the key parameters in controlling the wetting characteristics of a

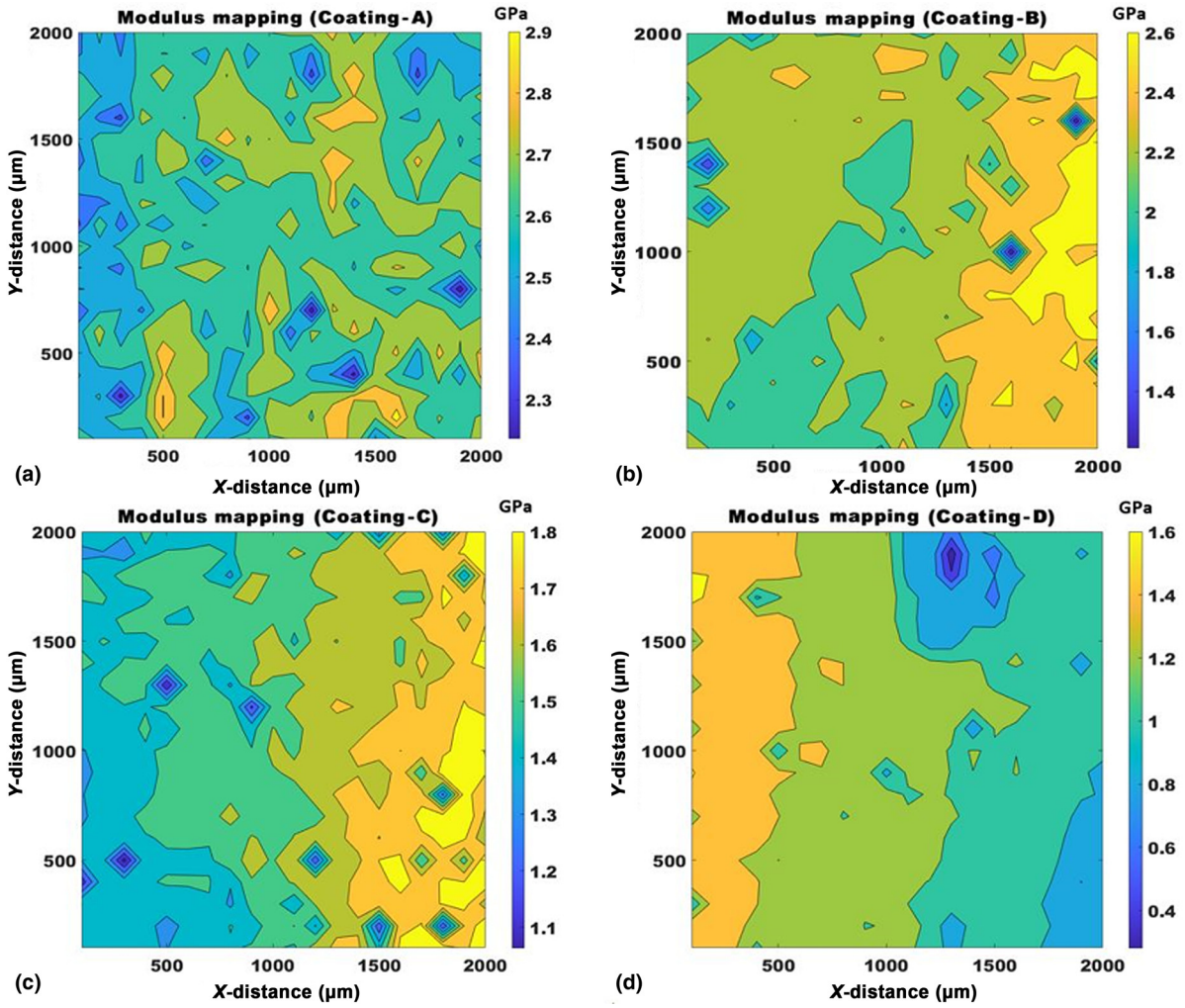

Figure 2. Reduced elastic modulus mapping for (a) coating-A, (b) coating-B, (c) coating-C, and (d) coating-D.

coating, the proportion should be balanced in order to reduce the surface free energy and simultaneously improve surface roughness. Figure 3 shows the variation in the static contact angle with respect to the amount of PDMS. As shown in Fig. 3, the maximum static contact angle was obtained for coating-B, where 1.0 g of PDMS was used along with 10 g of toluene and 1.5 g of silica nanoparticles. Static contact angles were measured for each nanocomposite coating, for which only the distinction was the amount of PDMS. The static contact angle corresponding to 0.5 g PDMS was 149°, and the contact angle was observed to increase up to 156° upon increasing the PDMS from 0.5 to 1.0 g. Upon further increasing the amount of PDMS to 1.5 g, a decline in the contact angle was observed, and the value was measured to be 145°. Finally, a steep decrease in the contact angle was observed after increasing the amount of PDMS to 2.0 g. The contact angle reduced to a very low value of 114°. The highest static contact angle observed for coating-B can be justified by the highest surface roughness observed in the case of coating-B among all the coatings. A detailed discussion about the surface morphology characteristics and its effect on surface wettability is presented in the following section. Supplementary Figure S1 shows the static contact angle image for a water droplet of 10 μL on coating-B.

Surface morphology analysis using atomic force microscopy

Figures 4(a)–(d) show the three-dimensional AFM images for coating-A, coating-B, coating-C, and coating-D. Supplementary Table S2 shows the statistical roughness parameters retrieved from the AFM images for all coatings. The statistical parameters measured from the AFM images include average roughness (R_A), root-mean-square roughness (R_{RMS}), surface skewness (R_{SK}), and kurtosis (R_{KU}). The surface roughness of any surface is often quantified by R_A and R_{RMS}, and those are the common parameters used for measuring surface roughness,[27,28] whereas, R_{SK} and R_{KU} are advanced roughness parameters that are not frequently given with basic surface

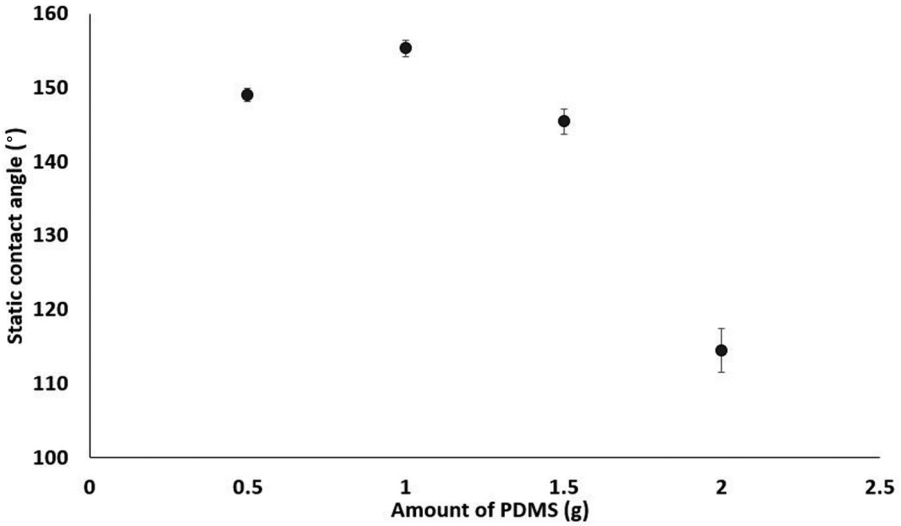

Figure 3. Variation in the static contact angle with respect to the amount of PDMS.

roughness measurements.[29–31] Surface skewness quantifies the symmetry of the statistical distribution of peaks and valleys in the surface topography of the sample. When the skewness value is 0, it means that the surface topography has equally distributed peaks and valleys of specific heights. Surface topography with more peaks than valleys indicates a positive surface skewness, whereas a negative surface skewness refers to more valleys than peaks in the surface topography. Kurtosis refers to

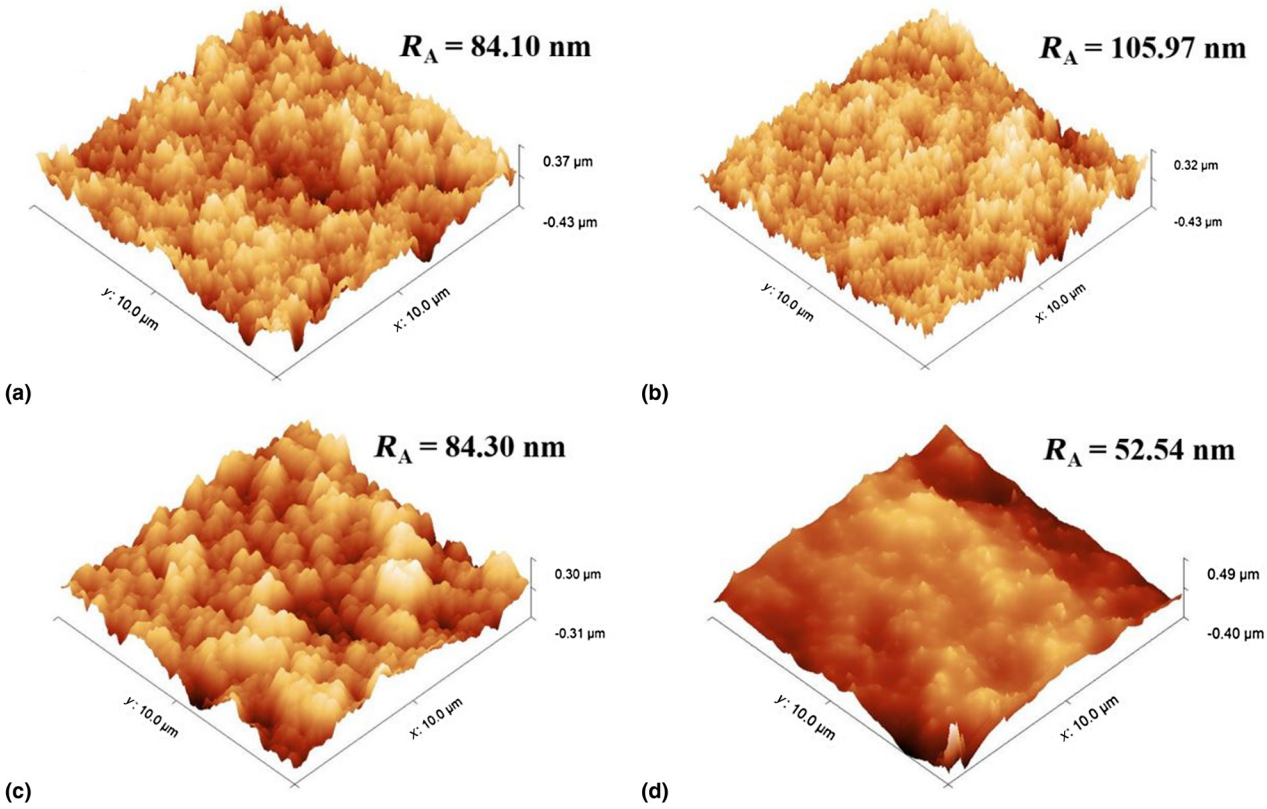

Figure 4. Three-dimensional AFM images for (a) coating-A, (b) coating-B, (c) coating-C, and (d) coating-D.

the probability density sharpness of the surface topography. For surfaces with low peaks and low valleys, kurtosis becomes less than 3, and for surfaces with high peaks and low valleys, it exceeds 3. The average surface roughness for coating-A, coating-B, coating-C, and coating-D was found to be 84.1 ± 2.2, 105.97 ± 4.8, 84.3 ± 3.3, and 52.54 ± 0.6 nm, respectively. The trend in variation of surface roughness is like the one observed in the case of static contact angle; hence, it is evident that the water contact angle is directly linked with the surface roughness characteristics of the coating. Coating-B showed the highest surface roughness of 105.97 nm, and in terms of static contact angle, coating-B also exhibited the highest value. Comparing coating-B, coating-C, and coating-D, the decrease in surface roughness observed as a result of increasing the amount of PDMS can be attributed to the possibility of the rough and dense silica structures partially or fully covered by the excess PDMS. The reason for coating-A to have lower surface roughness than coating-B could be insufficient binder within the nanocomposite coating solution to facilitate the formation of hierarchical silica structures. The surface skewness and kurtosis values reveal that the height distribution for all the coatings are much less skewed and hence highly symmetric, as the values for surface skewness lie between −0.5 and 0.5. Supplementary Figure S2 shows the representative scanning electron microscopy (SEM) image for the surface morphology alteration as a result of the nanocomposite coating.

Conclusion

In this work, the influence of the amount of PDMS binder within a nanocomposite solution on mechanical properties, surface wetting behavior, and surface roughness characteristics was studied. The results show that when the amount of PDMS binder is increased in the nanocomposite solution for a probable improvement in the mechanical properties of the coating, it compromises the required surface roughness requirements and hence the desired hydrophobicity. More importantly, contrary to the anticipated improvement in the mechanical properties as the amount of binder was increased, a decline in the mechanical properties was observed as the ratio between reinforcing nanoparticles and PDMS binder was reduced. The appropriate amount of PDMS binder with respect to the number of nanoparticles for this particular nanocomposite solution was found for achieving desired wetting behavior without compromising the mechanical properties and adherence onto the substrate.

Supplementary material

The supplementary material for this article can be found at https://doi.org/10.1557/mrc.2020.59.

Acknowledgments

This work was supported by the Center for Midstream Management and Science (CMMS) of Lamar University. The authors appreciate the Center for Innovation, Commercialization and Entrepreneurship (CICE) at Lamar University for providing lab space.

References

1. L. Xu, F. Liu, M. Liu, Z. Wang, Z. Qian, W. Ke, E. Han, G. Jie, J. Wang, and L. Zhu: Fabrication of repairable superhydrophobic surface and improved anticorrosion performance based on zinc-rich coating. *Prog. Org. Coat.* **137**, 105335 (2019).
2. C. Yao, D. Sebastian, I. Lian, Ö Günaydın-Şen, R. Clarke, K. Clayton, C. Chen, K. Kharel, Y. Chen, and Q. Li: Corrosion resistance and durability of superhydrophobic copper surface in corrosive NaCl aqueous solution. *Coatings* **8**, 70 (2018).
3. Z. Wang, Q. Li, Z. She, F. Chen, and L. Li: Low-cost and large-scale fabrication method for an environmentally-friendly superhydrophobic coating on magnesium alloy. *J. Mater. Chem.* **22**, 4097 (2012).
4. S. Jung, M. Dorrestijn, D. Raps, A. Das, C. Megaridis, and D. Poulikakos: Are superhydrophobic surfaces best for icephobicity? *Langmuir* **27**, 3059–3066 (2011).
5. X. Chen, Y. Chen, T. Jin, L. He, Y. Zeng, Q. Ma, and N. Li: Fabrication of superhydrophobic coating from non-fluorine siloxanes via a one-pot sol–gel method. *J. Mater. Sci.* **53**, 11253–11264 (2018).
6. J. Yu, L. Qin, Y. Hao, S. Kuang, X. Bai, Y. Chong, W. Zhang, and E. Wang: Vertically aligned boron nitride nanosheets: chemical vapor synthesis, ultraviolet light emission, and superhydrophobicity. *ACS Nano* **4**, 414–422 (2010).
7. H. Kahraman, I. Cevik, F. Dündar, and F. Ficici: The corrosion resistance behaviors of metallic bipolar plates for PEMFC coated with physical vapor deposition (PVD): an experimental study. *Arabian J. Sci. Eng.* **41**, 1961–1968 (2016).
8. D. Schaeffer, G. Polizos, D. Smith, D. Lee, S. Hunter, and P. Datskos: Optically transparent and environmentally durable superhydrophobic coating based on functionalized SiO_2nanoparticles. *Nanotechnology* **26**, 055602 (2015).
9. Z. Zhang, B. Ge, X. Men, and Y. Li: Mechanically durable, superhydrophobic coatings prepared by dual-layer method for anti-corrosion and self-cleaning. *Colloids Surf. A* **490**, 182–188 (2016).
10. Y. Qing, C. Yang, C. Hu, Y. Zheng, and C. Liu: A facile method to prepare superhydrophobic fluorinated polysiloxane/ZnO nanocomposite coatings with corrosion resistance. *Appl. Surf. Sci.* **326**, 48–54 (2015).
11. D. Sebastian, C. Yao, and I. Lian: Abrasion resistance of superhydrophobic coatings on aluminum using PDMS/SiO2. *Coatings* **8**, 414 (2018).
12. T. Wong, H. Wang, F. Wang, S. Sin, C. Quan, S. Wang, and X. Zhou: Development of a highly transparent superamphiphobic plastic sheet by nanoparticle and chemical coating. *J. Colloid Interface Sci.* **467**, 245–252 (2016).
13. Z. Chen, L. Hao, A. Chen, Q. Song, and C. Chen: A rapid one-step process for fabrication of superhydrophobic surface by electrodeposition method. *Electrochim. Acta* **59**, 168–171 (2012).
14. Z. She, Q. Li, Z. Wang, L. Li, F. Chen, and J. Zhou: Novel method for controllable fabrication of a superhydrophobic CuO surface on AZ91D magnesium alloy. *ACS Appl. Mater. Interfaces* **4**, 4348–4356 (2012).
15. D. Sebastian, C. Yao, and I. Lian: Multiscale corrosion analysis of superhydrophobic coating on 2024 aluminum alloy in a 3.5 wt% NaCl solution. *MRS Commun.* **10**, 305–311 (2020).
16. L. Xu, R. Karunakaran, J. Guo, and S. Yang: Transparent, superhydrophobic surfaces from one-step spin coating of hydrophobic nanoparticles. *ACS Appl. Mater. Interfaces* **4**, 1118–1125 (2012).
17. C. Cao, M. Ge, J. Huang, S. Li, S. Deng, S. Zhang, Z. Chen, K. Zhang, S. Al-Deyab, and Y. Lai: Robust fluorine-free superhydrophobic PDMS–ormosil@fabrics for highly effective self-cleaning and efficient oil–water separation. *J. Mater. Chem. A* **4**, 12179–12187 (2016).
18. D. Sebastian, C. Yao, and I. Lian: Mechanical durability of engineered superhydrophobic surfaces for anti-corrosion. *Coatings* **8**, 162 (2018).
19. S. Gao, X. Dong, J. Huang, S. Li, Y. Li, Z. Chen, and Y. Lai: Rational construction of highly transparent superhydrophobic coatings based on a non-particle, fluorine-free and water-rich system for versatile oil-water separation. *Chem. Eng. J.* **333**, 621–629 (2018).
20. T. Kim, J. Kim, and O. Jeong: Measurement of nonlinear mechanical properties of PDMS elastomer. *Microelectron. Eng.* **88**, 1982–1985 (2011).

21. R. Palchesko, L. Zhang, Y. Sun, and A. Feinberg: Development of polydimethylsiloxane substrates with tunable elastic modulus to study cell mechanobiology in muscle and nerve. *PLoS ONE* **7**, e51499 (2012).
22. K. Lei, K. Lee, and M. Lee: Development of a flexible PDMS capacitive pressure sensor for plantar pressure measurement. *Microelectron. Eng.* **99**, 1–5 (2012).
23. B. Bolvardi, J. Seyfi, I. Hejazi, M. Otadi, H. Khonakdar, and S. Davachi: Towards an efficient and durable superhydrophobic mesh coated by PDMS/TiO_2 nanocomposites for oil/water separation. *Appl. Surf. Sci.* **492**, 862–870 (2019).
24. S. Amirpoor, R. Siavash Moakhar, and A. Dolati: A novel superhydrophilic/superoleophobic nanocomposite PDMS-NH_2/PFONa-SiO_2 coated-mesh for the highly efficient and durable separation of oil and water. *Surf. Coat. Technol.* **394**, 125859 (2020).
25. M.K. Srinath and M.S. Ganesha Prasad: Surface morphology and hardness analysis of TiCN coated AA7075 aluminium alloy. *J. Inst. Eng. (India): Series C* **100**, 221–228 (2019).
26. Z. Wang, A.A. Volinsky, and N.D. Gallant: Nanoindentation study of polydimethylsiloxane elastic modulus using Berkovich and flat punch tips. *J. Appl. Polym. Sci.* **132**, 1–7 (2015).
27. T. Young, J. Jackson, S. Roy, H. Ceylan, and S. Sundararajan: Tribological behavior and wettability of spray-coated superhydrophobic coatings on aluminum. *Wear*, 376–377 (2017).
28. X. Zhang, J. Mo, Y. Si, and Z. Guo: How does substrate roughness affect the service life of a superhydrophobic coating? *Appl. Surf. Sci.* **441**, 491–499 (2018).
29. A. Khaskhoussi, L. Calabrese, and E. Proverbio: Superhydrophobic self-assembled silane monolayers on hierarchical 6082 aluminum alloy for anti-corrosion applications. *Appl. Sci.* **10**, 2656 (2020).
30. S. Sutha, R. Kumar, B. Raj, and K. Ravi: Ultrasonic-assisted fabrication of superhydrophobic ZnO nanowall films. *Bull. Mater. Sci.* **40**, 505–511 (2017).
31. S. Naderizadeh, S. Dante, P. Picone, M. Di Carlo, R. Carzino, A. Athanassiou, and I. Bayer: Bioresin-based superhydrophobic coatings with reduced bacterial adhesion. *J. Colloid Interface Sci.* **574**, 20–32 (2020).